Research Article | Vol. 28, No. 4 / 17 February 2020 / Optics Express 5875

Optics EXPRESS

Flat cholesteric liquid crystal polymeric lens with low f-number

YANNANQI LI,[1,2] TAO ZHAN,[1,2] AND SHIN-TSON WU[1,*]

[1]College of Optics and Photonics, University of Central Florida, Orlando, FL 32816, USA
[2]These authors contributed equally to this work
[*]swu@creol.ucf.edu

Abstract: We use a simple photoalignment method to fabricate four reflective cholesteric liquid crystal (CLC) polymeric lenses with diameter D=2.45 cm and low f-numbers (f/2, f/0.9, f/0.45, f/0.33) at 550 nm. Such a flat CLC lens can be converging or diverging, depending on the handedness and direction of the incident light. Our CLC lenses can achieve ~85% diffraction efficiency for a designated polarization state and manifest decent imaging ability.

1. Introduction

The Pancharatnam-Berry phase [1,2], also known as geometric phase, can be conveniently realized by spatially patterning the liquid crystal (LC) director orientations. Such a spatial-varying phase change (φ) is twice the optic axis orientation angle θ of the LC director in-plane acquired by the polarized light. Based on this principle, various optical elements have been demonstrated, such as gratings [3–5], vortex waveplates [6–8], lenses [9–14] and so on. These novel Pancharatnam-Berry optical elements (PBOEs) have found widespread applications in lighting [15], displays [16], telescopy [17] and beam steering [18,19], just to name a few. Among these optical elements, planar PB lens (PBL) attracts considerable interest because its lensing effect originates from the spatial-varying optical anisotropy instead of conventional optical path length difference. The focal length can be expressed by the Fresnel's approximation as $f = \pi r^2/\lambda\varphi$, where r is the lens radius, λ is the wavelength used in the imaging system, and φ is the phase difference between the center and the lens edge. Both transmissive and reflective PBOEs have been developed. The fabrication methods include nano-rubbing [20], lithography [21], polarization holography [22,23], and direct laser writing [9]. The f-number of a lens is defined as f/#=f/D, where f is the focal length and D is the diameter of the effective aperture. With a larger collection cone, low f/# lenses can benefit both imaging and display systems with higher light efficiency. For a conventional lens, a straightforward way to reduce f/# is to enlarge the lens curvature, which leads to a bulkier structure. Therefore, how to achieve low f/# while keeping thin lens profile is urgently needed.

Extensive efforts have focused on developing transmissive PBL with a low f/#. In 2015, a broadband high diffraction efficiency (99%) PBL with f/2.3 at λ=633 nm has been reported [9]. Afterwards, several transmissive PBLs with lower f/# have been developed. By using the polarization holography and direct-write photo-alignment technique, an ultra-thin (~2.26 μm) PBL with f/2.1 (at 633 nm) and an f/1.5 lens with high achromatic efficiency have been demonstrated [10,11]. For transmissive PBLs, further reducing the f/# is quite challenging because it is difficult to achieve decent LC alignment for the areas with high spatial frequency. More recently, a reflective lens cell with 1-mm diameter and 20.3-cm focal length was demonstrated using a patterned CLC [12]. However, the calculated f/# is larger than 200. To overcome the limited f/# issue of transmissive PBLs, here we demonstrate a record-low f/# diffractive lens by adopting the CLC structure.

In this paper, we demonstrate four flat on-axis reflective CLC lenses with different f-numbers (f/2, f/0.9, f/0.45, f/0.33 at 550 nm) fabricated using the optical imprinting technique [24].

#387942 https://doi.org/10.1364/OE.387942
Journal © 2020 Received 10 Jan 2020; revised 9 Feb 2020; accepted 9 Feb 2020; published 14 Feb 2020

Optics EXPRESS

With the same lens diameter (D=2.45 cm), the corresponding focal length is approximately 4.9 cm, 2.2 cm, 1.1 cm and 0.8 cm (at λ=550 nm), respectively. Without using the sophisticated holographic exposure setup, our fabrication process is much simpler and less sensitive to the ambient turbulence. The CLC lenses produced in this process exhibit good quality with a reasonably high reflection efficiency. To the best of our knowledge, this is the first demonstration of high-quality reflective polymeric CLC lenses with such a low f/#. The reported flat thin-film reflective lenses can be used as an optical combiner in augmented reality system for widening the field-of-view, and as a compact polarization-selective lens in catadioptric virtual reality viewing optics.

2. Working principles

Figure 1(a) depicts the LC anisotropy axis orientation distribution of the reflective lens with patterned CLC from top view, while the cross-sectional view is shown in Fig. 1(b). The corresponding phase change is generically plotted in Fig. 1(c). For a transmissive PBL, the sign of optical power is dependent on the polarization handedness and direction of the incident light. But for our reflective CLC lens, due to its polarization selectivity, the right-handed circularly polarized (RCP) light will be reflected by the right-handed CLC, while the left-handed circularly polarized (LCP) component will pass through the lens. Figures 1(d) and 1(e) illustrate different lensing effects of the incident light coming from different sides. Here, symbol '+' stands for positive optical power for the RCP light, while '-' represents negative optical power for the RCP light. When an unpolarized light is incident from the '+' side (Fig. 1(d)), due to the polarization selective reflectivity, the RCP light is reflected and converged, while the LCP light passes through without being affected. On the other hand, when an unpolarized light is incident from the '-' side (Fig. 1(e)), the RCP light is reflected and diverged, while the LCP light passing through directly without any effect.

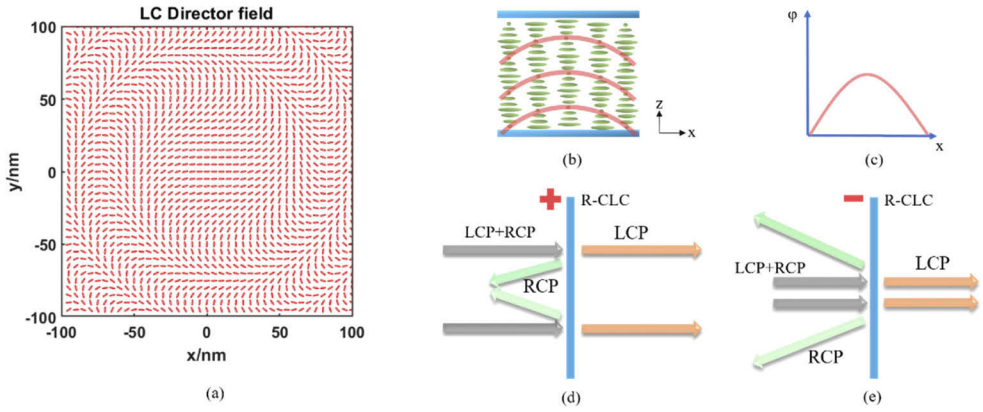

Fig. 1. (a) Schematic distribution of LC anisotropy axis orientation from top view. (b) The CLC structure of cross-sectional view. (c) The corresponding phase profile along x-axis. Lensing behaviors of a CLC lens with (d) positive power and (e) negative power.

3. Device fabrication

To fabricate the optical elements with specific patterns, a commonly employed method is polarization holography [9]. In such method, fabricating a low f/# lens usually needs a template lens with lower f/#. However, due to the existence of the bulky beam splitter, it is difficult to fabricate such a short focal length, while maintaining a large diameter because the exposure plane is behind the beam splitter. Compared to the conventional polarization holography approach, our

Optics EXPRESS

imprinting technique is more reliable due to its insensitivity to ambient perturbation. Another distinguished advantage is that without using the complex holographic setup, a CLC lens with much smaller f-number can be achieved.

In experiment, our first step to fabricate the reflective CLC lens is to spin-coat a photo-alignment layer onto cleaned glass substrates. We used Brilliant Yellow (BY) as the photo-alignment material, which was dissolved in dimethylformamide (DMF) solution with a concentration of 0.4% by weight. To create uniform thin films on the substrates, we controlled the spin-coating speed at 500 rpm for 5 s and then 3,000 rpm for 30 s. Then, the films were dried for 30 minutes on a hotplate at 120 °C. Next, the substrates were exposed under a linearly polarized light (λ=457nm). The polarization direction of the exposure light is perpendicular to the aligning direction of the photo-alignment layer.

Figure 2 depicts the exposure system. The laser used is Cobolt Twist 457nm. After spatial filtering and beam expansion, the collimated linearly polarized light was used as incident light. Here, we could choose a transmissive PBL or a set of PBLs as the master lenses, behind which our glass substrates were placed and exposed for about 5 minutes at an intensity of ~6 mW/cm^2. By stacking multiple PBLs as master lenses, we could obtain different focal lengths with the same diameter. Here, we need to emphasize the importance of high (~100%) first-order diffraction efficiency of the master PBL. Only under such condition, the zero-order light leakage can be completely suppressed, so that high-quality lens pattern can be achieved. Otherwise, some unwanted ghost images would be inevitable. In our experiment, the master transmissive PBLs (f/4, f/1.8 at 550 nm, D=2.45 cm) were purchased from Edmund Optics.

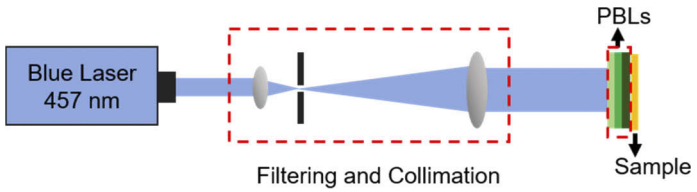

Fig. 2. The optical setup of the exposure system. The master PBLs are transmissive. The sample is the glass substrate coated with Brilliant Yellow photo-alignment material.

After exposure, we spin-coated the CLC polymer onto the patterned surface so the LC molecules would follow the generated patterns on the photo-alignment layer. The detailed fabrication process is illustrated in Fig. 3. The CLC polymer precursor consists of 93.85wt% RM257, 2.15wt% R5011, 3wt% Irgacure651, and 1% surfactant Zonyl 8857A. By adding a small amount of surfactant, the film surface quality will be improved, leading to better molecular alignment and fewer defects. The reflection efficiency is highly dependent on the CLC film thickness. The film thickness is determined by the dilution of CLC precursor in tolune and the rotating speed of the spin-coater. The lower dilution and slower rotating speed will lead to a thicker film. To achieve high efficiency, the precursor was diluted in toluene at 1:2.5 by weight and then spin-coated onto the exposed substrates at 3000 rpm for 30 s. And the coated substrate was cured with UV light (λ≈365 nm and power density ≈ 7 mW/cm^2) for 5 minutes in nitrogen environment which leads to a crossed-link polymer.

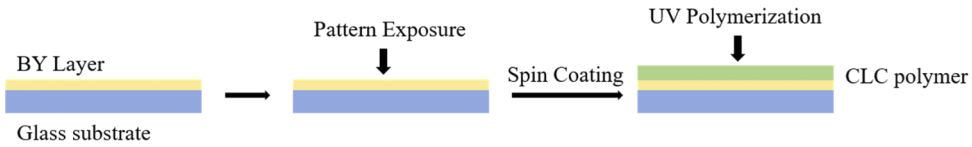

Fig. 3. Schematic illustration of fabrication procedures of the polymeric CLC lens.

Optics EXPRESS

In order to fabricate reflective CLC lenses with f/2, f/0.9, f/0.45, and f/0.33 at λ=550 nm, we chose transmissive PBLs with different f-numbers to stacked them together as the master lenses. For the input linearly polarized light, after passing through a half-wave plate oriented at angle, the phase change becomes φ ($\varphi = 2\theta$). And the focal length of imprinted pattern can be approximately twice as short as that of the master PBL with the same diameter and same wavelength used in the imaging system. Therefore, f/2 and f/0.9 CLC lenses can be fabricated by imprinting one PBL with f/4 and f/1.8, respectively. Considering the limited f-number availability of the PBL, it is difficult to fabricate a lens with f-number lower than one. Thus, to imprint CLC lenses with shorter focal length, we could stack multiple PBLs to generate different f-numbers according to $k = k_1 + k_2 - k_1 k_2 d$, where k_1 is the optical power of the first PBL, k_2 is the optical power of the second PBL, d is the thickness between the stacking PBLs, and k is the total optical power for the master PBLs. To stack more PBLs, the same equation can also be applied. Compared to the focal lengths that are several centimeters long, the thickness d (1~2 mm) of the stacked PBL can be ignored. Thus, in order to fabricate the f/0.45 and f/0.33 CLC lenses, we stacked two f/1.8 PBLs and three f/1.8 PBLs together, respectively.

4. Results and discussion

Figures 4(a)–4(d) show the photographs of our fabricated reflective CLC lenses with different f-numbers. The images observed are the ceiling fluorescent lamps in our labs. The lens surfaces are quite clear and uniform, except for few defects. Because these four lenses have same diameter (D = 2.45 cm), a lower f/# leads to a smaller image.

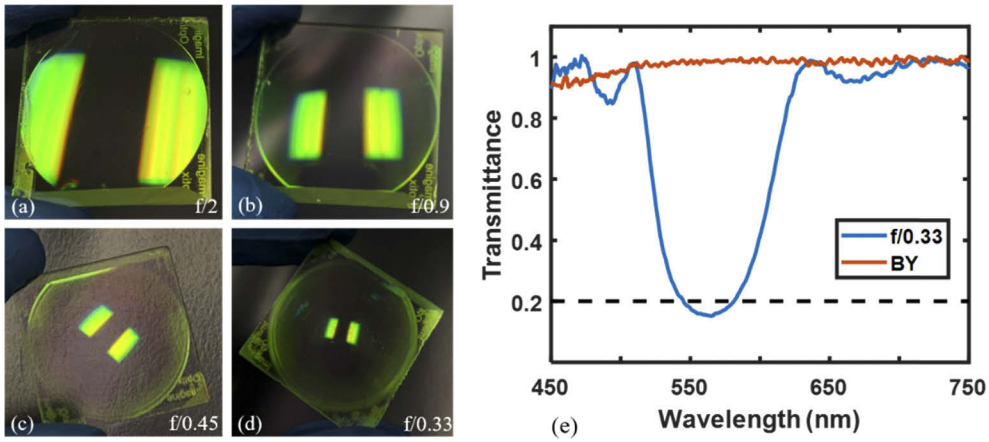

Fig. 4. Photographs of the fabricated CLC lenses (D=2.45 cm) with (a) f/2; (b) f/0.9; (c) f/0.45; (d) f/0.33. (e) Measured transmission spectrum of the f/0.33 CLC lens and a glass substrate coated with a thin layer of Brilliant Yellow photo-alignment material.

To get a decent transmittance of our sample, we used a glass substrate coated with Brilliant Yellow as reference to normalize the spectrum. Firstly, we put the reference glass substrate in a spectrometer with RCP as incident light to serve as normalized transmittance. Then we placed the sample in the spectrometer and measured the transmittance at normal angle. Figure 4(e) depicts the measured transmission spectra of the f/0.33 CLC lens and a glass substrate coated with a thin layer of the photo-alignment material. When measuring BY transmission spectrum, a clear glass substrate was used as reference to normalize the spectrum. In our experiment, only 0.4% BY was dissolved. Under such condition, a little absorption in blue region will be observed but it will not affect the lens performance and the reflection efficiency. For the transmission spectrum of CLC lens, within the reflection band, the transmittance is around 15%. Outside this

Optics EXPRESS

band, the transmittance shows almost 100% in the visible spectral region, which indicates both scattering and absorption losses are extremely small. The reflection efficiency is about 85% for the RCP light. As mentioned above, the reflection efficiency depends on the film thickness in order to establish Bragg reflection. For the different f-number lenses we fabricated, they show almost the same efficiency with the same CLC polymer precursor, indicating the similar film thickness. By measuring the efficiency at different positions of the sample, they show almost no variation, confirming good uniformity of the lens. The spectral bandwidth of the lens depends on the birefringence of the employed LC polymer. To dynamically switch the polymeric lens, we need to add a polarization rotator, as will be discussed later.

Figures 5(a)–5(h) represent the polarizing optical microscope images of our CLC lenses with different magnification around the center. As shown in Figs. 5(a)–5(d), under 5X magnification, as the f-number gets smaller, the grating period becomes shorter and more lens fringes are observed. The grating period is defined as LC director changes 180° along the direction of radius. Detailed results reveal our fabricated CLC lenses exhibiting good molecular alignment with clear pattern and very few defects, which may come from the dusts in the air. These small defects will not considerably degrade the imaging quality of the lens. Here, we need to emphasize on the CLC alignment structure. For such a high spatial frequency, it is challenging to keep the *nematic* LC directors well aligned on the top interface due to the high volume free energy. In this case, LC directors on the top interface tend to be homeotropic, leading to defects. But regarding the *cholesteric* LC structure, with the help of chiral dopant, the volume free energy of twist structure is zero, which contributes to better alignment even on the top interface. More detailed analysis of LC molecular dynamic has been discussed in [25].

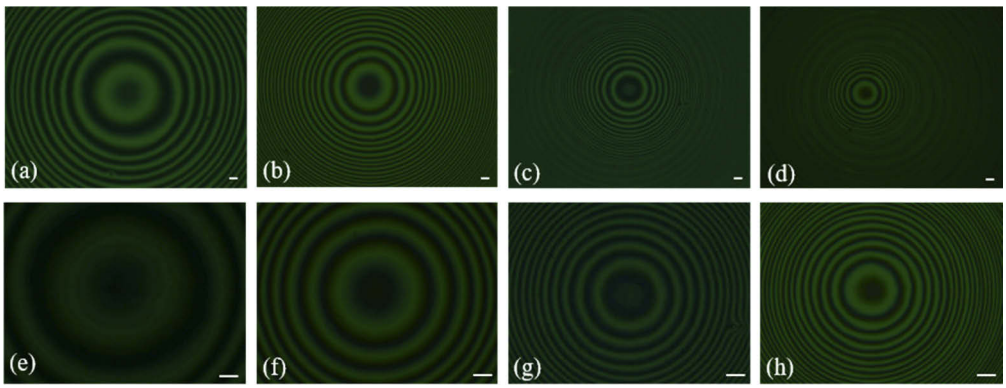

Fig. 5. Polarizing optical microscope images of the CLC lenses under 5x and 10x magnification with f/2 [(a), (e)], f/0.9 [(b), (f)], f/0.45 [(c), (g)], and f/0.33 [(d), (h)]. Scale bars: 50 μm.

We used 1951 USAF resolution target to test the image quality. The measurement system is shown in Fig. 6(a). The resolution target is illuminated by a green LED incorporated with a 550-nm band-pass filter whose full width at half maximum (FWHM) is 10 nm. In order to produce uniform incident light, a diffuser film was placed in front of the light source. Since it is an on-axis reflective lens, a beam splitter (BS) after the resolution target is needed to observe the image. We placed the CLC lens on one side of the BS and a camera on the opposite side to capture the image. Figures 6(b)–6(d) show the resolution target images of the CLC lenses with f/0.9 and f/0.45. The samples were positioned within one focal distance to generate upright and magnified images for clear observation. Figure 6(b) shows the sharp lines of Groups 2 and 3 for the CLC lens with f/0.9, and Fig. 6(c) shows the enlarged part of Fig. 6(b). We could resolve Group 5 Element 1, which is 32 lp/mm. For the lower f/# CLC lens, the focal length

Optics EXPRESS

is too short to be put within one focal distance because of the beam splitter. Thus, to see the image of the f/0.45 lens, we put the lens directly in front of the resolution target by eliminating the beam splitter. In this case, the image can be observed directly on the other side. However, as Fig. 6(d) shows, besides the enlarged Group 4 and Group 5, there are some magnified lines in the peripheral areas. These are caused by the multiple reflections of the images.

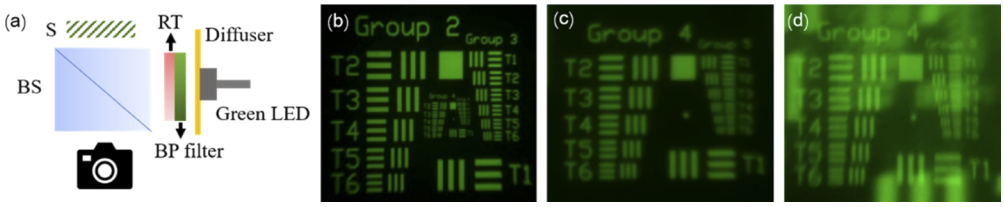

Fig. 6. (a) Optical setup for testing resolution. BS: beam splitter; S: CLC lens sample; RT: resolution target; BP filter: band-pass filter. (b)–(d) Observed images of the CLC lenses (D=2.45 cm) by using a 10-nm FWHM band-pass filter in front of the green LED ($\lambda \approx 550$ nm). (b) f/0.9; (c) Enlarged Group 4 of (b); (d) f/0.45.

Finally, we illustrate a potential application of these reflective CLC lenses for compact multi-plane display in an augmented reality system. As Fig. 7 depicts, the proposed display system consists of a high resolution LCD, a polarization rotator and a quarter-wave plate. The polarization rotator is designed to achieve full-range modulation between two orthogonal polarization states (0° and 90°). After passing through the QWP, the outgoing image can be considered either RCP or LCP. These circularly polarized beams will be reflected by the CLC lens with the corresponding handedness after passing through the beam splitter. The CLC lenses are designed to have different optical powers for two different circular polarization states. Under such condition, the reflected images will have two focal depths due to different optical power of the CLC lenses. Such a design can mitigate the vergence-accommodation conflict issue in an augmented reality system as demonstrated in [26], yet with a much smaller footprint.

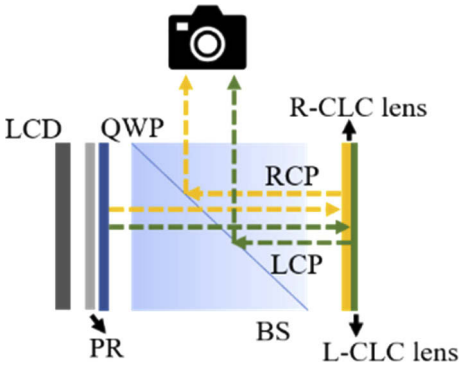

Fig. 7. The proposed multi-plane display system. PR: polarization rotator; BS: beam splitter; QWP: quarter-wave plate. The dashed yellow lines represent the optical path of the right-handedness CLC lens and the green lines are for the left-handedness CLC lens. The two optical paths can be differentiated due to the different focal lengths of two CLC lenses.

5. Conclusion

We have fabricated several low f-numbers reflective CLC lenses with diameter D=2.45 cm by using imprinting technology. Without sophisticated holographic setup, the fabrication process is

Optics EXPRESS

much simpler and low f-number lenses can be achieved. These lenses exhibit a reasonably high reflection efficiency and good image quality.

Funding

Intel Corporation; Air Force Office of Scientific Research (FA9550-14-1-0279).

Disclosures

The authors declare no conflicts of interest.

References

1. S. Pancharatnam, "Generalized theory of interference, and its application," Proc. - Indian Acad. Sci., Sect. A **44**(5), 247–262 (1956).
2. J. Anandan, "The geometric phase," Nature **360**(6402), 307–313 (1992).
3. C. Oh and M. J. Escuti, "Achromatic diffraction from polarization gratings with high efficiency," Opt. Lett. **33**(20), 2287–2289 (2008).
4. K. Gao, C. McGinty, H. Payson, S. Berry, J. Vornehm, V. Finnemeyer, B. Roberts, and P. Bos, "High-efficiency large-angle Pancharatnam phase deflector based on dual-twist design," Opt. Express **25**(6), 6283–6293 (2017).
5. A. Ryabchun and A. Bobrovsky, "Cholesteric liquid crystal materials for tunable diffractive optics," Adv. Opt. Mater. **6**(15), 1800335 (2018).
6. S. C. McEldowney, D. M. Shemo, R. A. Chipman, and P. K. Smith, "Creating vortex retarders using photoaligned liquid crystal polymers," Opt. Lett. **33**(2), 134–136 (2008).
7. D. Mawet, E. Serabyn, K. Liewer, C. Hanot, S. McEldowney, D. Shemo, and N. O'Brien, "Optical vectorial vortex coronagraphs using liquid crystal polymers: theory, manufacturing and laboratory demonstration," Opt. Express **17**(3), 1902–1918 (2009).
8. P. Chen, L. L. Ma, W. Duan, J. Chen, S. J. Ge, Z. H. Zhu, M. J. Tang, R. Xu, W. Gao, T. Li, W. Hu, and Y. Q. Lu, "Digitalizing self-assembled chiral superstructures for optical vortex processing," Adv. Mater. **30**(10), 1705865 (2018).
9. J. Kim, Y. Li, M. N. Miskiewicz, C. Oh, M. W. Kudenov, and M. J. Escuti, "Fabrication of ideal geometric-phase holograms with arbitrary wavefronts," Optica **2**(11), 958–964 (2015).
10. K. Gao, H.-H. Cheng, A. K. Bhowmik, and P. J. Bos, "Thin-film Pancharatnam lens with low f-number and high quality," Opt. Express **23**(20), 26086–26094 (2015).
11. K. J. Hornburg, J. Kim, and M. J. Escuti, "Experimental characterization of a F/1.5 geometric-phase lens with high achromatic efficiency and low aberration," Proc. SPIE **10125**, 101250Y (2017).
12. J. Kobashi, H. Yoshida, and M. Ozaki, "Planar optics with patterned chiral liquid crystals," Nat. Photonics **10**(6), 389–392 (2016).
13. T. Zhan, J. Zou, J. Xiong, X. Liu, H. Chen, J. Yang, S. Liu, Y. Dong, and S. T. Wu, "Practical chromatic aberration correction in virtual reality displays enabled by large-size ultra-broadband liquid crystal polymer lenses," Adv. Opt. Mater. **8**(8), 1901360 (2020).
14. Z. Zhou, Y. Guo, H. Yu, M. Jiang, T. Turiv, I. Chaganava, O. D. Lavrentovich, and Q. H. Wei, "Liquid crystal Pancharatnam-Berry optical elements," Proc. SPIE **11092**, 11 (2019).
15. F. Snik, M. Rodenhuis, M. J. Escuti, L. Brickson, K. Hornburg, J. Kim, C. Kievid, S. Groenhuijsen, and D. Roosegaarde, "Producing true-color rainbows with patterned multi-layer liquid-crystal polarization gratings," Opt. Mater. Express **9**(4), 1583–1589 (2019).
16. T. Zhan, Y. H. Lee, G. Tan, J. Xiong, K. Yin, F. Gou, J. Zou, N. Zhang, D. Zhao, J. Yang, S. Liu, and S. T. Wu, "Pancharatnam-Berry optical elements for head-up and near-eye displays [invited]," J. Opt. Soc. Am. B **36**(5), D52–D65 (2019).
17. B. Piccirillo, E. Piedipalumbo, L. Marrucci, and E. Santamato, "Electrically tunable vector vortex coronagraphs based on liquid-crystal geometric phase waveplates," Mol. Cryst. Liq. Cryst. **684**(1), 15–23 (2019).
18. J. Kim, C. Oh, S. Serati, and M. J. Escuti, "Wide-angle, nonmechanical beam steering with high throughput utilizing polarization gratings," Appl. Opt. **50**(17), 2636–2639 (2011).
19. F. Gou, F. Peng, Q. Ru, Y. H. Lee, H. Chen, Z. He, T. Zhan, K. L. Vodopyanov, and S. T. Wu, "Mid-wave infrared beam steering based on high-efficiency liquid crystal diffractive waveplates," Opt. Express **25**(19), 22404–22410 (2017).
20. M. Honma and T. Nose, "Polarization-independent liquid crystal grating fabricated by microrubbing process," Jpn. J. Appl. Phys. **42**(Part 1, No. 11), 6992–6997 (2003).
21. Z. Bomzon, V. Kleiner, and E. Hasman, "Space-variant polarization state manipulation with computer-generated subwavelength metal stripe gratings," Opt. Commun. **192**(3-6), 169–181 (2001).
22. C. Provenzano, P. Pagliusi, and G. Cipparrone, "Highly efficient liquid crystal based diffraction grating induced by polarization holograms at the aligning surfaces," Appl. Phys. Lett. **89**(12), 121105 (2006).

Optics EXPRESS

23. T. Zhan, J. Xiong, Y. H. Lee, R. Chen, and S. T. Wu, "Fabrication of Pancharatnam-Berry phase optical elements with highly stable polarization holography," Opt. Express **27**(3), 2632–2642 (2019).
24. S. R. Nersisyan, N. V. Tabiryan, D. M. Steeves, and B. R. Kimball, "Characterization of optically imprinted polarization gratings," Appl. Opt. **48**(21), 4062–4067 (2009).
25. J. Xiong, R. Chen, and S. T. Wu, "Device simulation of liquid crystal polarization gratings," Opt. Express **27**(13), 18102–18112 (2019).
26. Q. Chen, Z. Peng, Y. Li, S. Liu, P. Zhou, J. Gu, J. Lu, L. Yao, M. Wang, and Y. Su, "Multi-plane augmented reality display based on cholesteric liquid crystal reflective films," Opt. Express **27**(9), 12039–12047 (2019).